Supplement of Atmos. Chem. Phys., 17, 5561–5581, 2017
http://www.atmos-chem-phys.net/17/5561/2017/
doi:10.5194/acp-17-5561-2017-supplement

Atmospheric Chemistry and Physics Open Access EGU

Supplement of

How can mountaintop CO_2 observations be used to constrain regional carbon fluxes?

John C. Lin et al.

Correspondence to: John C. Lin (john.lin@utah.edu)

Fig. S1

Three-dimensional plots of the terrain over a domain of ~$1^{o}\times1^{o}$ surrounding the NWR site, as resolved by the WRF 1.3-km model. The NWR site is indicated by the triangle. A small subsample of the numerous stochastic trajectories simulated by STILT, driven by WRF started at 2100 UTC (1400 MST), are drawn as black lines. Also shown is the average back trajectory (pink), derived by averaging locations of the stochastic trajectories. In addition, the PBL heights averaged along the backtrajectory are shown as the blue line.

Adjusting the CT-2013b diurnal cycle

In the CarbonTracker assimilation process, attempts to match CO_2 observations could result in "dipoles" in scaling factors between nearby ecoregions, leading to negative fluxes even at night (Fig. S2a). While respiration can occur during the day when vegetation is under stress (e.g., droughts), photosynthetic uptake (negative fluxes) at night, in the absence of sunlight, is biologically unphysical. In order to correct the reversed diurnal cycle seen in CarbonTracker, a reversal had to be first detected within CarbonTracker for the selected grid cell for a given day. Once the reversal was detected, the sign of the biospheric flux was flipped. The positive flux was then adjusted so that the net flux for the selected gridcell for the given day was equal to 0. Finally, the negative flux was adjusted so that the final net flux was equal to the original net flux, which preserved the total net flux for the day (Fig. S3). The resulting biosperic flux pattern can seen in Fig. S2b.

Fig. S2

Mean biospheric fluxes from Jun~Aug 2012 averaged between 0600~0900 UTC (2300~0200 MST). (a) Biospheric fluxes for the unmodified CarbonTracker flux fields and (b) biospheric fluxes for the adjusted CarbonTracker flux fields. The black circle represents HDP, the black diamond represents SPL, and the black star represents NWR.

Fig. S3

Schematic showing the adjustment of erroneous diurnal pattern in biospheric flux within CarbonTracker (red line), with nighttime uptake, to a corrected biospheric flux (green line). The dashed line represents a flux of 0.

Fig. S4

Average contributions to CO_2 variations at HDP, SPL, and NWR from biospheric, anthropogenic, and wildfire fluxes at different times of the day between Jun~Aug 2012 as simulated by STILT, driven with WRF-1.3km winds. Also shown are the observed variations, calculated by subtracting out the STILT-derived background (see Sect. 2.3).

Fig. S5

Time series of CO_2 errors (Simulated – Observed) at the HDP, SPL, and NWR sites during the study period (Jun~Aug 2012) for the different model configurations—i.e., WRF-1.3km AGL, 4-km AGL, 12-km AGL, and GDAS-ASL. The thin lines denote CO_2 errors calculated at high frequency, at 3-hourly time spacing. The thick lines represent the CO_2 errors smoothed with a 4-day centered running average that will be correlated with other meteorological variables (Table S1). The bias and root-mean-square error (RMSE) reported on the top-right hand box are calculated based on the 3-hourly time series. The gap in the earlier part of July at NWR is due to missing observations.

Fig. S6

Mean CO_2 concentrations extracted from the bottom 8 levels of CarbonTracker, in the respective gridcells where the HDP, SPL, and NWR sites are located. The mean model heights of the bottom 8 levels are (in meters AGL): 25, 103, 247, 480, 814, 1259, 1822, 2508. The concentrations interpolated to the heights of the 3 sites are indicated by the orange dashed line. The observed values are drawn in black, with unfiltered data (dashed) and after applying the filter for removing local influences (solid; Sect. 2.1).

Fig. S7

The average footprint (shown in $\log_{10}$) for the SPL at 0200 MST (0900 UTC), gridded at $0.1^o \times 0.1^o$. The site is denoted as a triangle. The average back trajectory (averaged over the stochastic STILT trajectories) is drawn as a line, with points indicating trajectory locations every hour, as the trajectory moves back from the site indicated as points. Magenta parts of the trajectory refer to the nighttime (1900~0700 MST), while pink portions indicate the daytime (0700~1900 MST). Parts of the trajectory are shaded with blue when it is found below the average height of the PBL along the trajectory.

Fig. S8

Similar to Fig. S7, but for 1400 MST (2100 UTC).

Fig. S9

Similar to Fig. S7, but for the NWR site.

Fig. S10

Similar to Fig. S9, but for 1400 MST (2100 UTC).

Fig. S11

Three dimensional plots of the terrain over a domain of ~1^{o}×1^{o} surrounding HDP, as resolved by the WRF and GDAS models at various grid spacings. Also shown is the average back trajectory, derived by averaging locations of the numerous stochastic trajectories simulated by STILT, driven by the various WRF meteorological fields and the global GDAS field. Back trajectories were started from HDP at 1400 MST (2100 UTC). Points indicate trajectory locations every hour, as the trajectory moves back from the site indicated as points. Magenta portions of the trajectory refer to the nighttime (1900~0700 MST), while pink portions indicate the daytime (0700~1900 MST). In addition, the PBL heights averaged along the backtrajectory are shown as the blue line.

Fig. S12

Similar to Fig. S11, but for SPL.

Fig. S13

Similar to Fig. S11, but for NWR.

Table S1

Correlation coefficients between CO_2 errors smoothed with a 4-day centered running average (Fig. S5) and potential explanatory meteorological variables observed near the HDP, SPL, and NWR sites. The smoothing window of 4-days was selected to focus on synoptic scale meteorological changes. The meteorological observations come from radiosondes launched at 00-UTC and 12-UTC from the following airports: Salt Lake City, Grand Junction, and Denver for the HDP, SPL, and NWR sites, respectively. The meteorological variables are extracted at the 500-hPa level and include the observed geopotential height (GPH), geopotential height gradient between NWR and HDP (NWR – HDP), observed windspeed, as well as the U- and V- components of the observed wind vector. The GPH time series is processed by subtracting its 20-day running average (centered) to remove trends and seasonal variations and then smoothed with a 4-day running average. Pearson correlation coefficients are reported here; coefficients with lower statistical significance (p>0.05) are not shown and indicated with "-" in the Table.

	HDP				**SPL**				**NWR**			
	WRF 1.3-km	*WRF 4-km*	*WRF 12-km*	*GDAS*	*WRF 1.3-km*	*WRF 4-km*	*WRF 12-km*	*GDAS*	*WRF 1.3-km*	*WRF 4-km*	*WRF 12-km*	*GDAS*
GPH	0.35	0.57	-	0.39	-	-	0.17	-	-	-	-	-0.19
GPH gradient	-0.37	-0.39	-	-	0.20	0.25	0.57	-	-0.71	-0.69	-0.64	-0.66
U wind	-	-	-0.30	-	0.60	0.64	0.54	0.49	0.30	0.33	0.20	0.37
V wind	-0.53	-0.49	-	-	-	0.19	0.49	0.24	-0.52	-0.52	-0.44	-0.49
Windspeed	-0.16	-0.24	-0.18	-	0.43	0.49	0.59	0.34	-	-	-	-

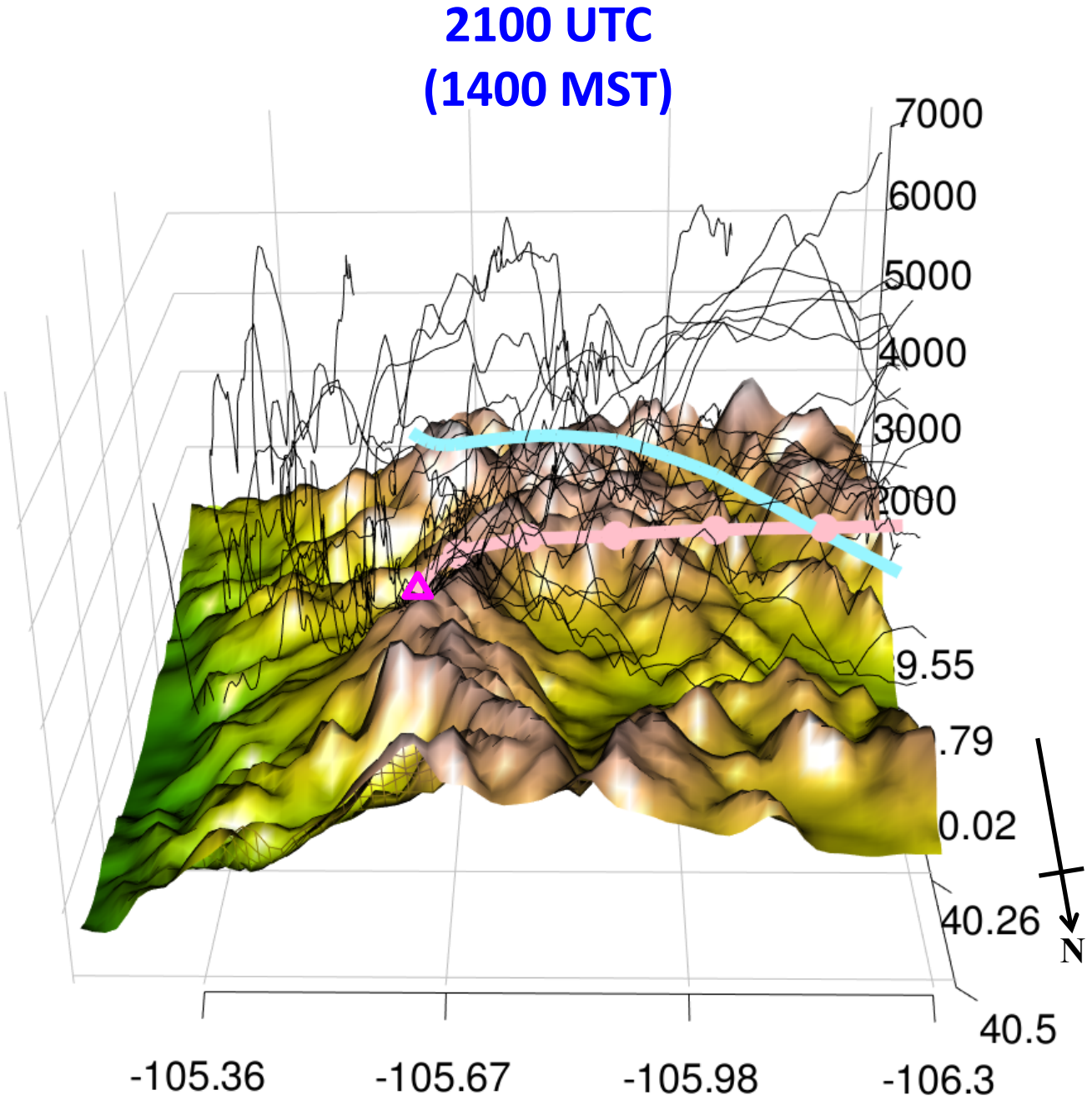
2100 UTC
(1400 MST)
7000
6000
5000
4000
3000
2000
9.55
.79
0.02
40.26
N
40.5
-105.36
-105.67
-105.98
-106.3

Fig. S1

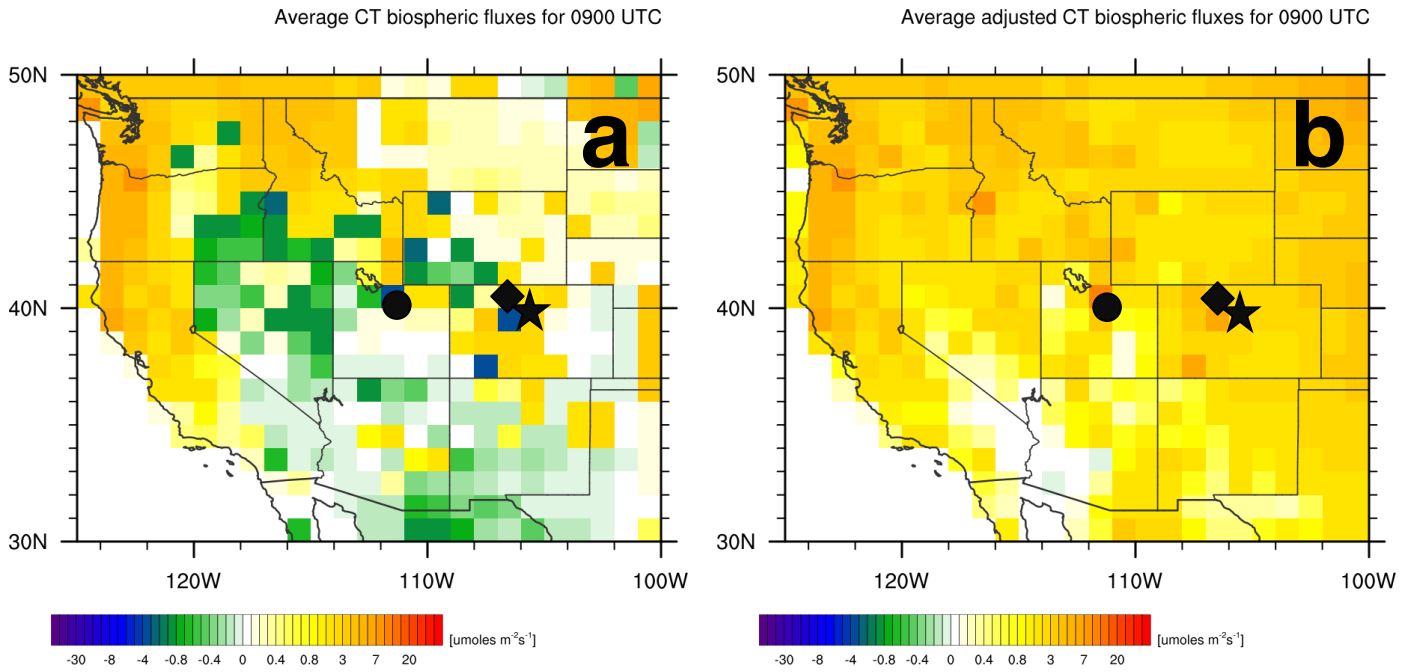
Average CT biospheric fluxes for 0900 UTC
Average adjusted CT biospheric fluxes for 0900 UTC
a
b
50N
40N
30N
120W
110W
100W
-30 -8 -4 -0.8 -0.4 0 0.4 0.8 3 7 20
[umoles m-2s-1]

Fig. S2

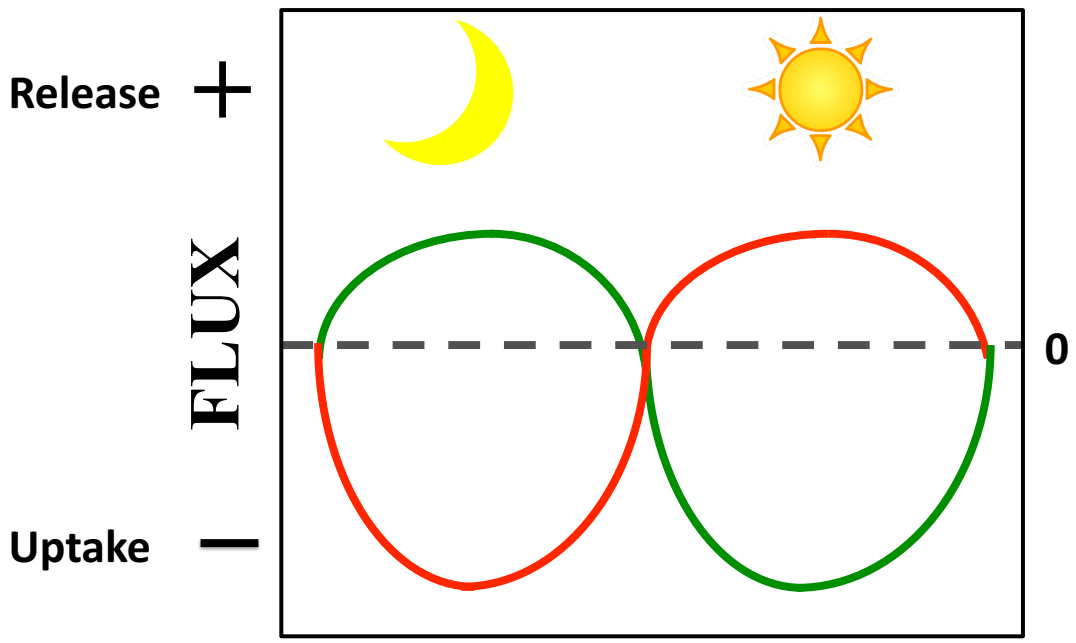

Fig. S3

Average Diurnal Contributions from Different CO_2 Sources

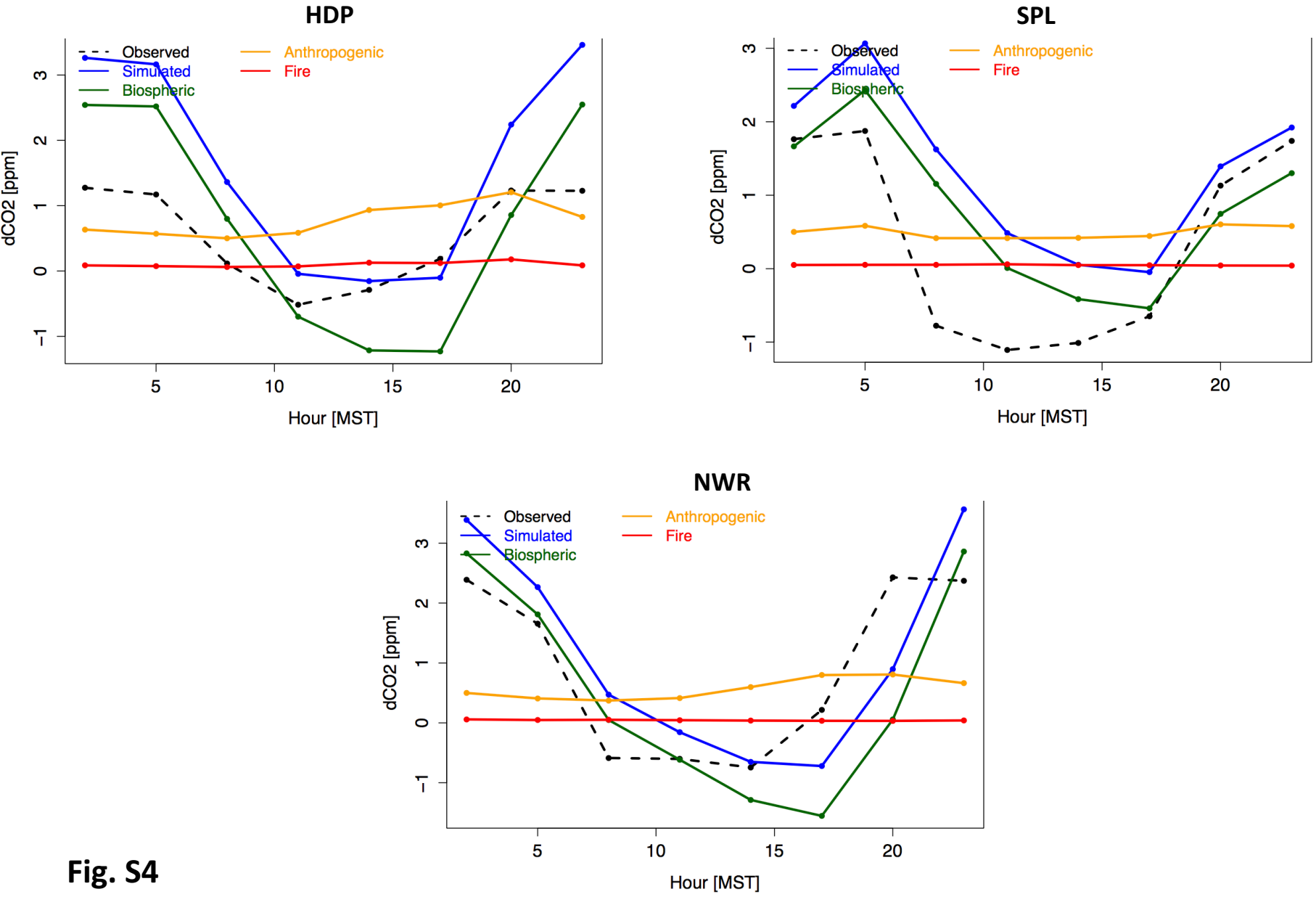

Fig. S4

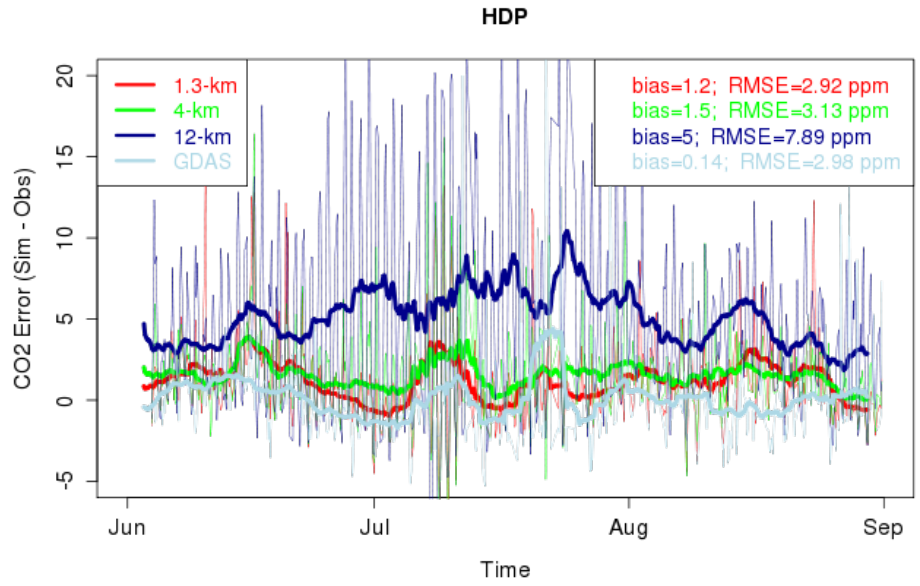
HDP
1.3-km
4-km
12-km
GDAS
bias=1.2; RMSE=2.92 ppm
bias=1.5; RMSE=3.13 ppm
bias=5; RMSE=7.89 ppm
bias=0.14; RMSE=2.98 ppm
CO2 Error (Sim - Obs)
Jun
Jul
Aug
Sep
Time

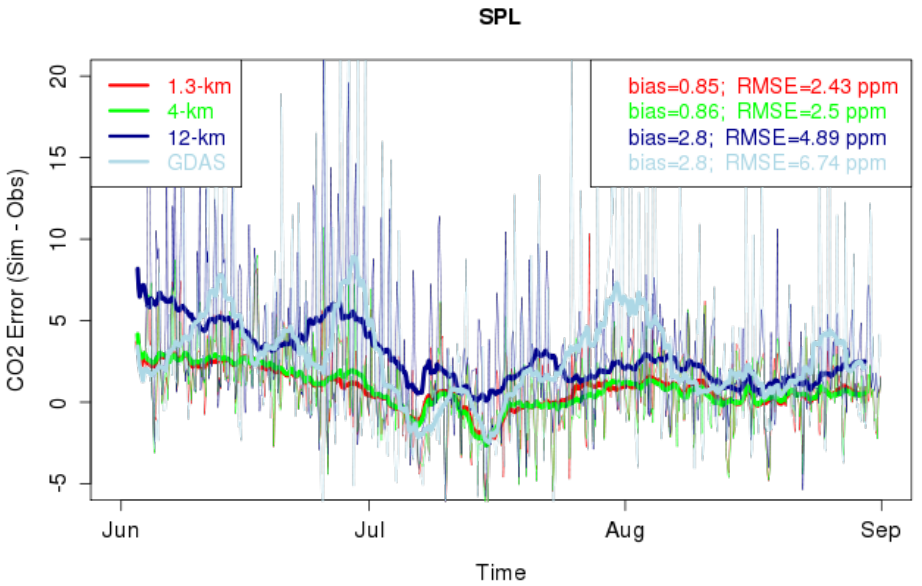
SPL
1.3-km
4-km
12-km
GDAS
bias=0.85; RMSE=2.43 ppm
bias=0.86; RMSE=2.5 ppm
bias=2.8; RMSE=4.89 ppm
bias=2.8; RMSE=6.74 ppm
CO2 Error (Sim - Obs)
Jun
Jul
Aug
Sep
Time

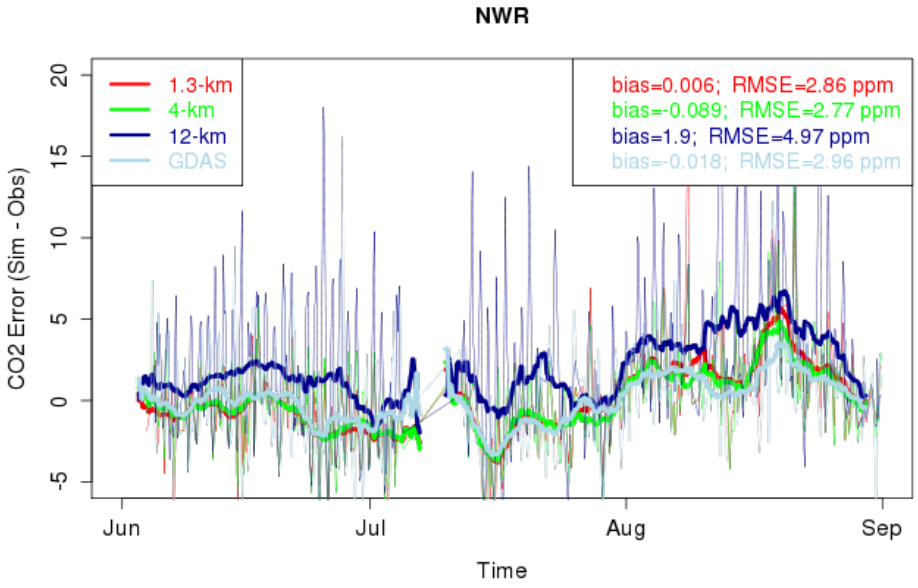
NWR
1.3-km
4-km
12-km
GDAS
bias=0.006; RMSE=2.86 ppm
bias=-0.089; RMSE=2.77 ppm
bias=1.9; RMSE=4.97 ppm
bias=-0.018; RMSE=2.96 ppm
CO2 Error (Sim - Obs)
Jun
Jul
Aug
Sep
Time

Fig. S5

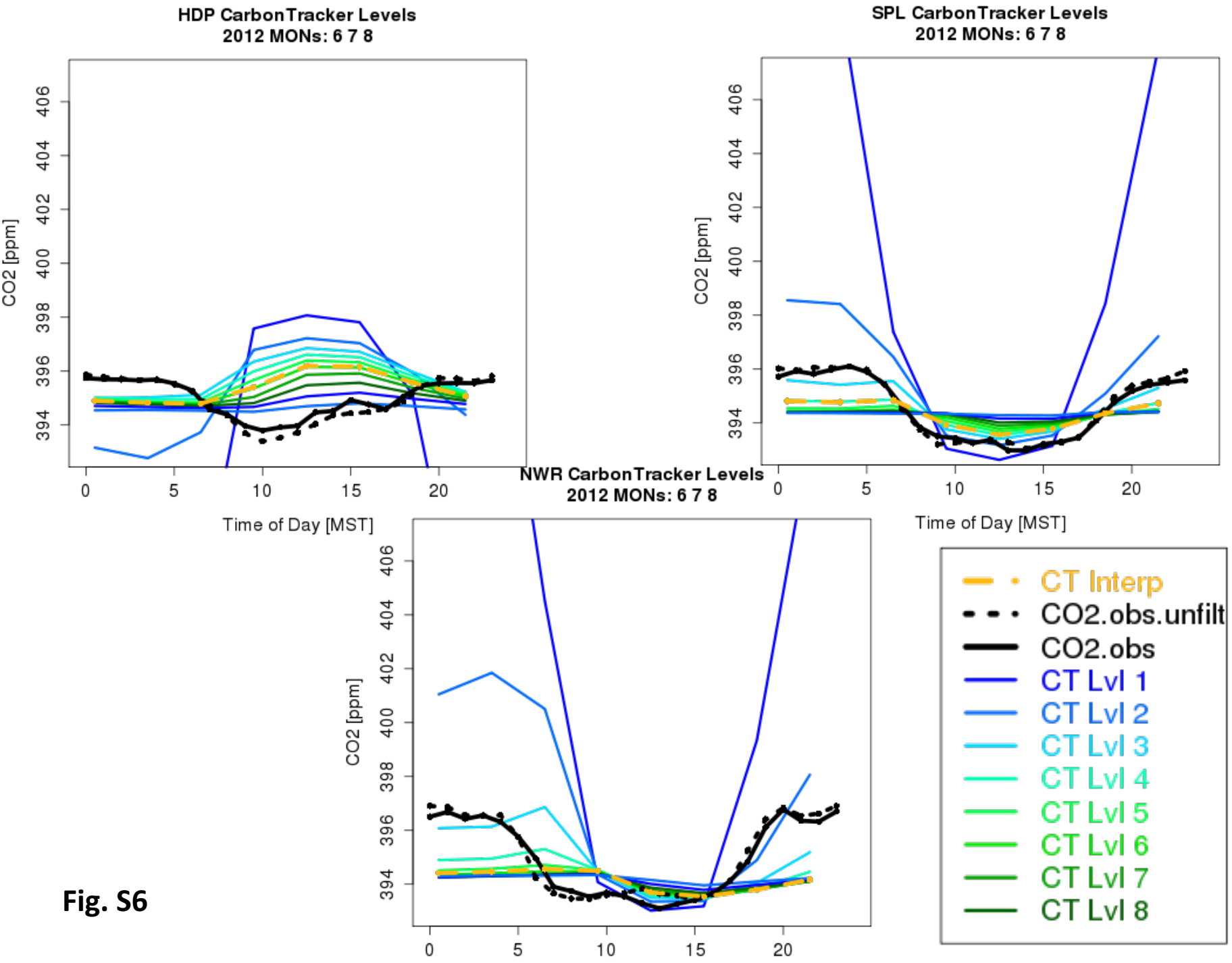
HDP CarbonTracker Levels
2012 MONs: 6 7 8
SPL CarbonTracker Levels
2012 MONs: 6 7 8
NWR CarbonTracker Levels
2012 MONs: 6 7 8
CO2 [ppm]
Time of Day [MST]
394
396
398
400
402
404
406
0
5
10
15
20
CT Interp
CO2.obs.unfilt
CO2.obs
CT Lvl 1
CT Lvl 2
CT Lvl 3
CT Lvl 4
CT Lvl 5
CT Lvl 6
CT Lvl 7
CT Lvl 8

Fig. S6

SPL ave footprint: WRF-1.3km (AGL)

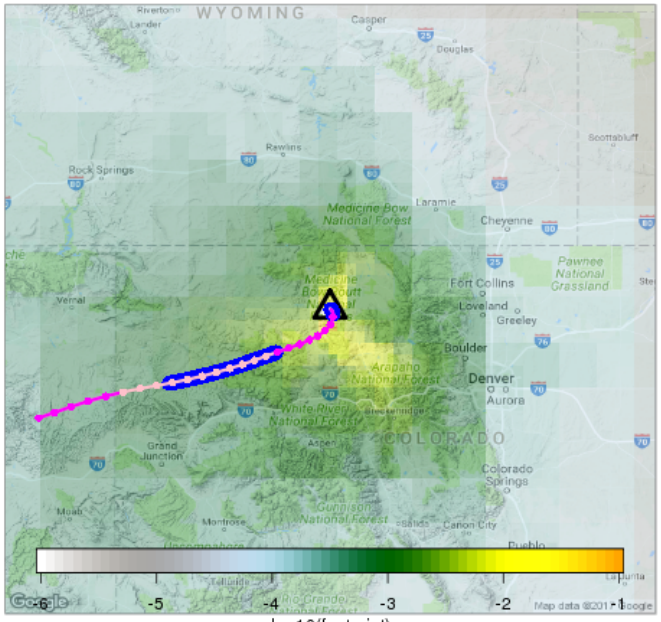

SPL ave footprint: WRF-4km (AGL)

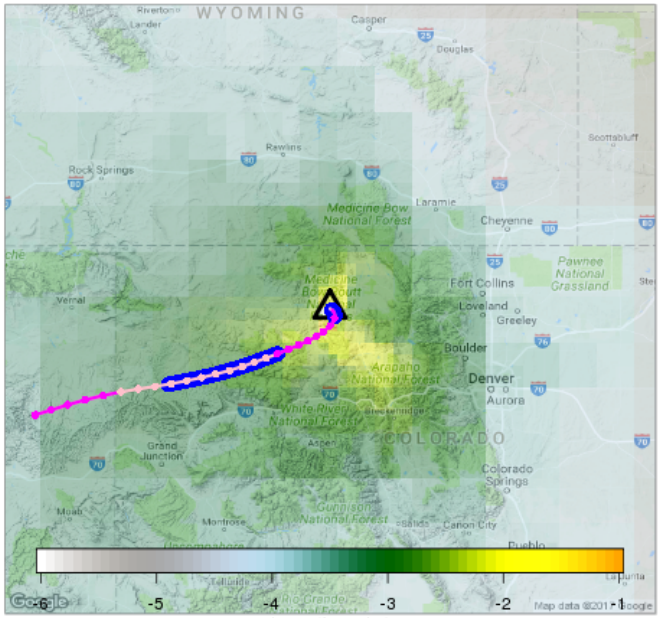

0900 UTC (0200 MST)

Nighttime (1900~0700 MST)

Daytime (0700~1900 MST)

Trajectory in PBL

SPL ave footprint: WRF-12km (AGL)

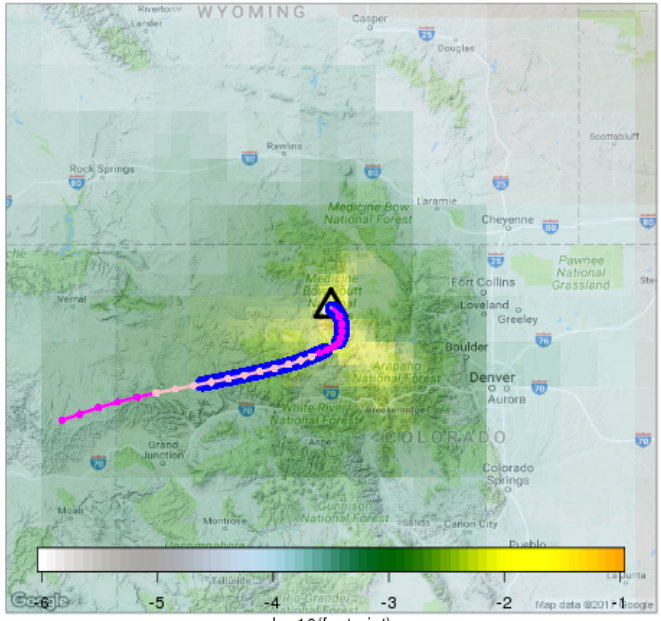

SPL ave footprint: GDAS-1° (ASL)

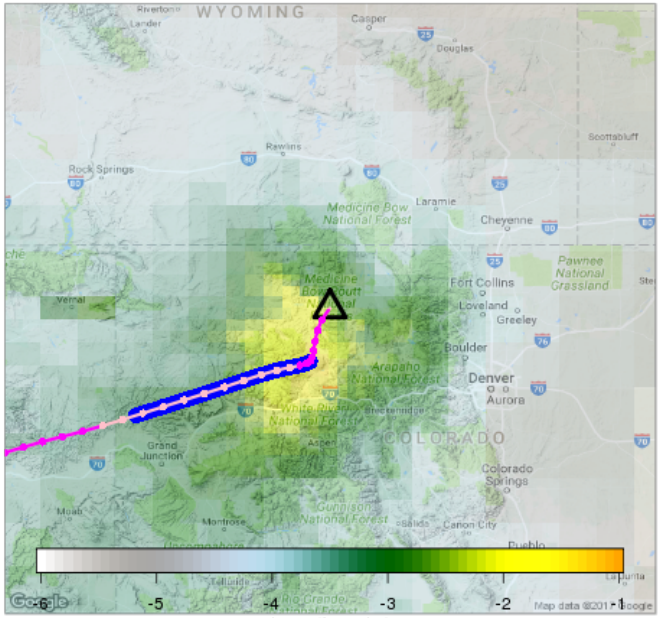

Fig. S7

SPL ave footprint: WRF-1.3km (AGL)

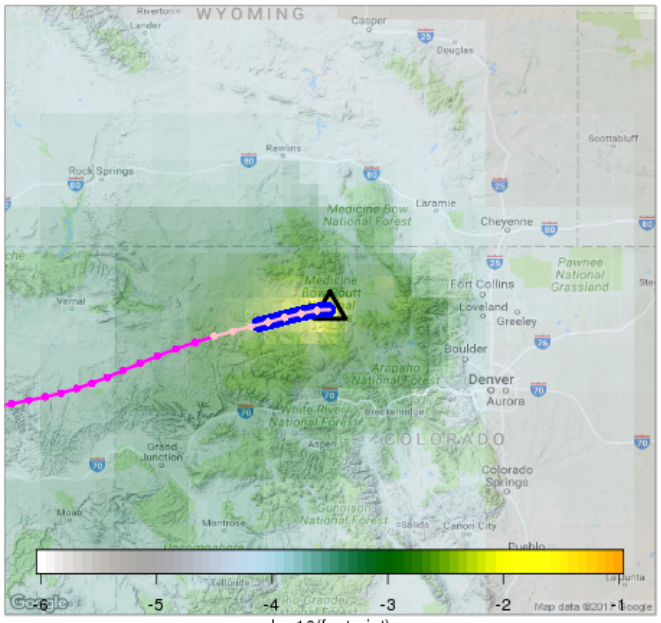

SPL ave footprint: WRF-4km (AGL)

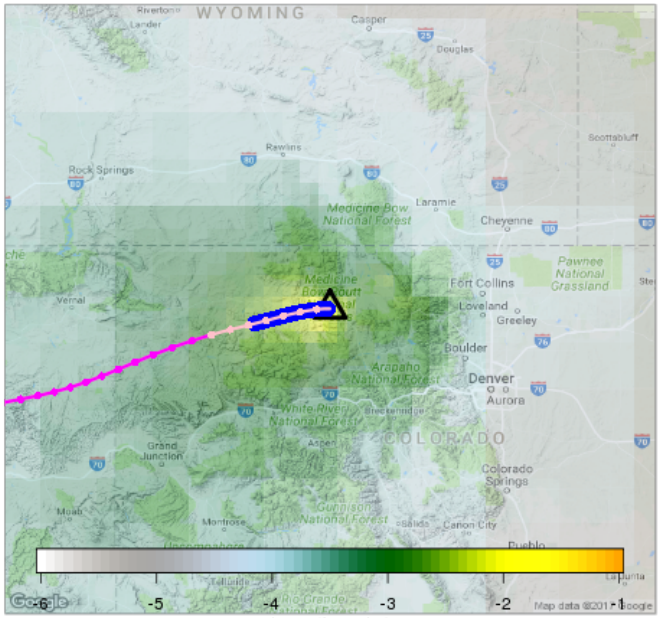

2100 UTC
(1400 MST)

Nighttime
(1900~0700 MST)

Daytime
(0700~1900 MST)

Trajectory in
PBL

SPL ave footprint: WRF-12km (AGL)

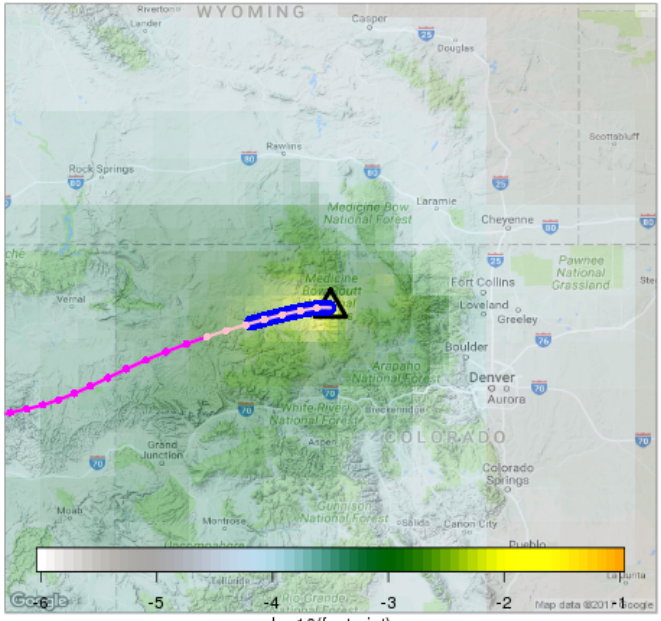

SPL ave footprint: GDAS-1° (ASL)

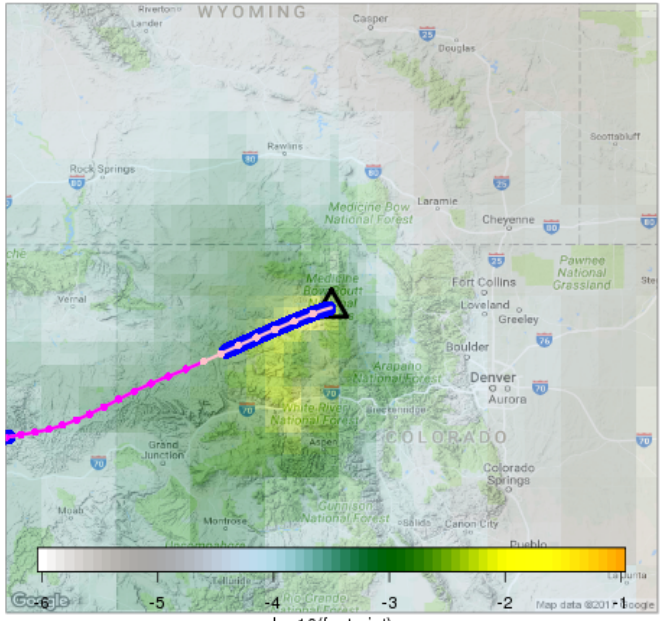

Fig. S8

NWR ave footprint: WRF-1.3km (AGL)

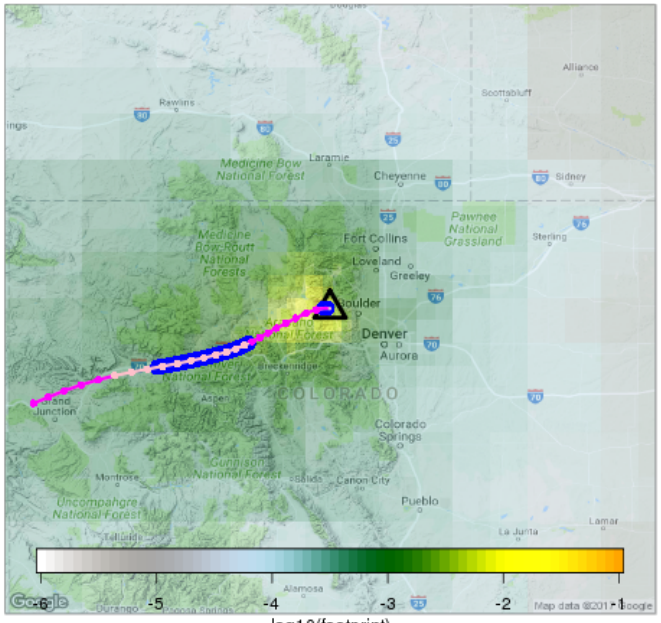

NWR ave footprint: WRF-4km (AGL)

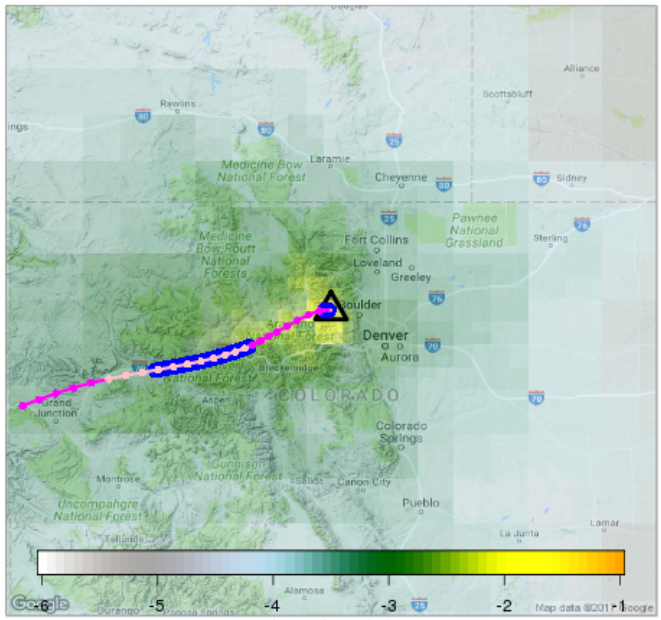

0900 UTC
(0200 MST)

Nighttime
(1900~0700 MST)

Daytime
(0700~1900 MST)

Trajectory in
PBL

NWR ave footprint: WRF-12km (AGL)

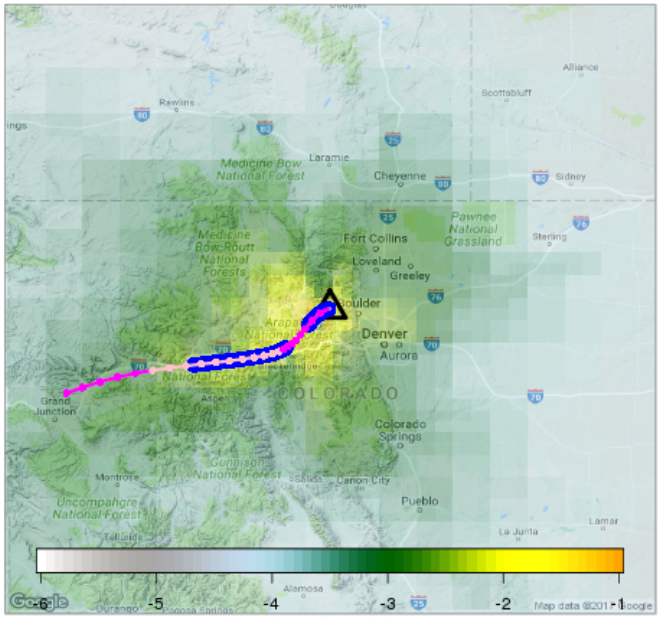

NWR ave footprint: GDAS-1° (ASL)

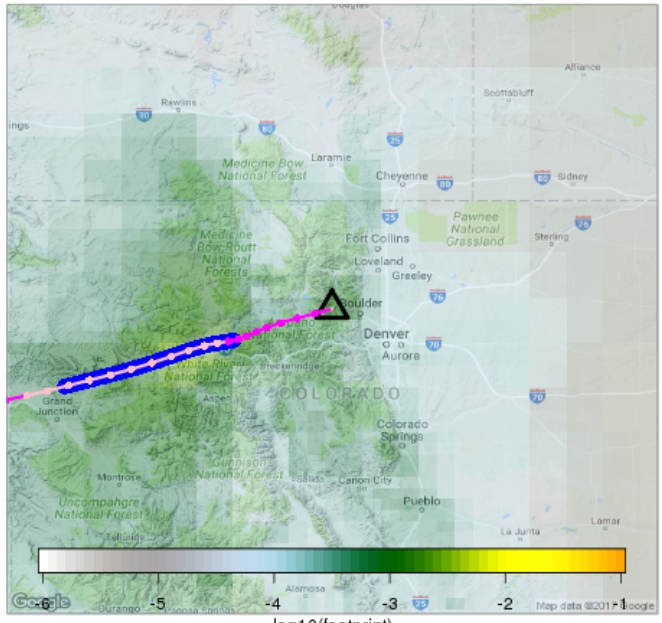

Fig. S9

NWR ave footprint: WRF-1.3km (AGL)

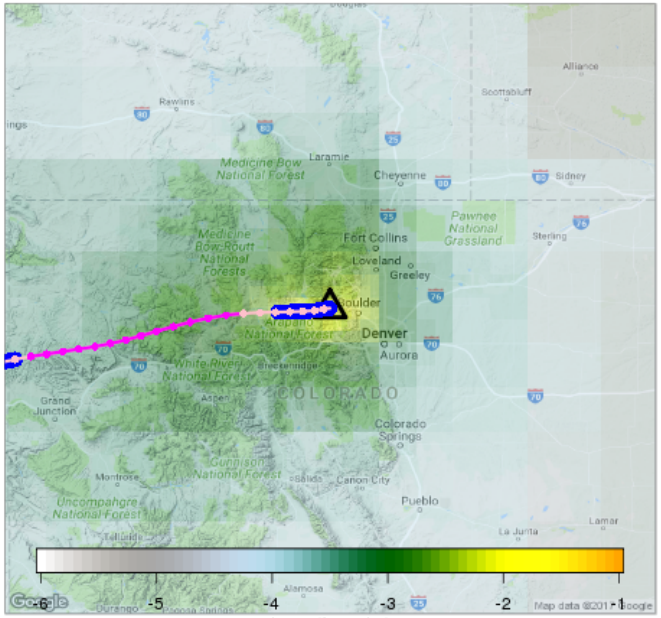

NWR ave footprint: WRF-4km (AGL)

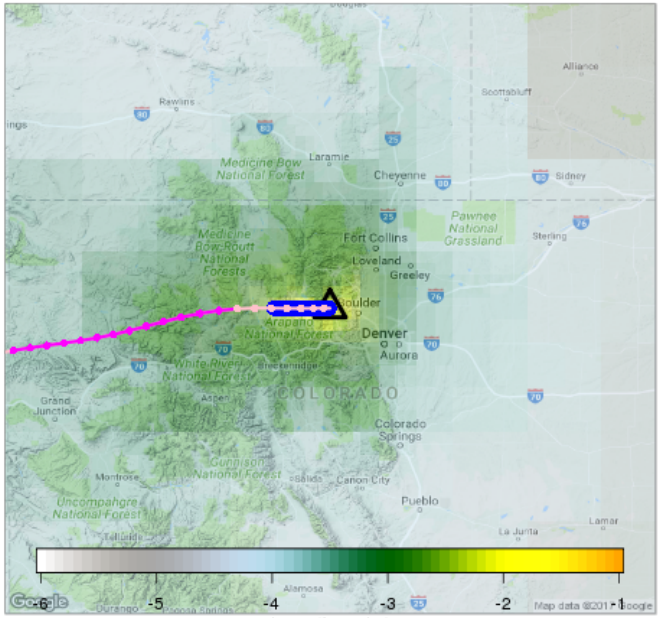

2100 UTC (1400 MST)

Nighttime (1900~0700 MST)

Daytime (0700~1900 MST)

Trajectory in PBL

NWR ave footprint: WRF-12km (AGL)

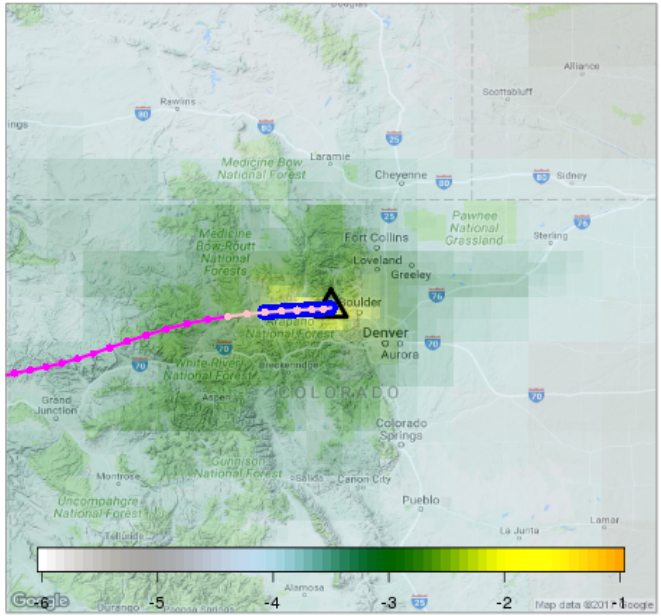

NWR ave footprint: GDAS-1° (ASL)

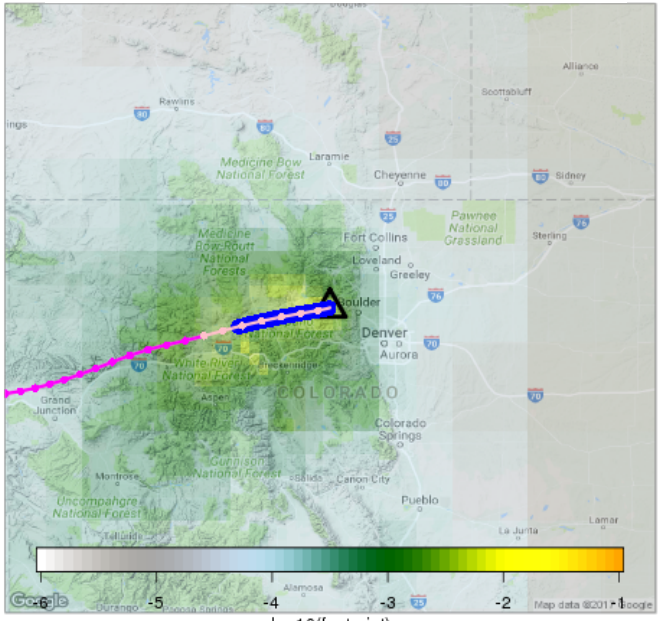

Fig. S10

HDP: Mean 3D Trajectory of Stochastic Particles & PBL ht for Different Runs

2100 UTC (1400 MST)

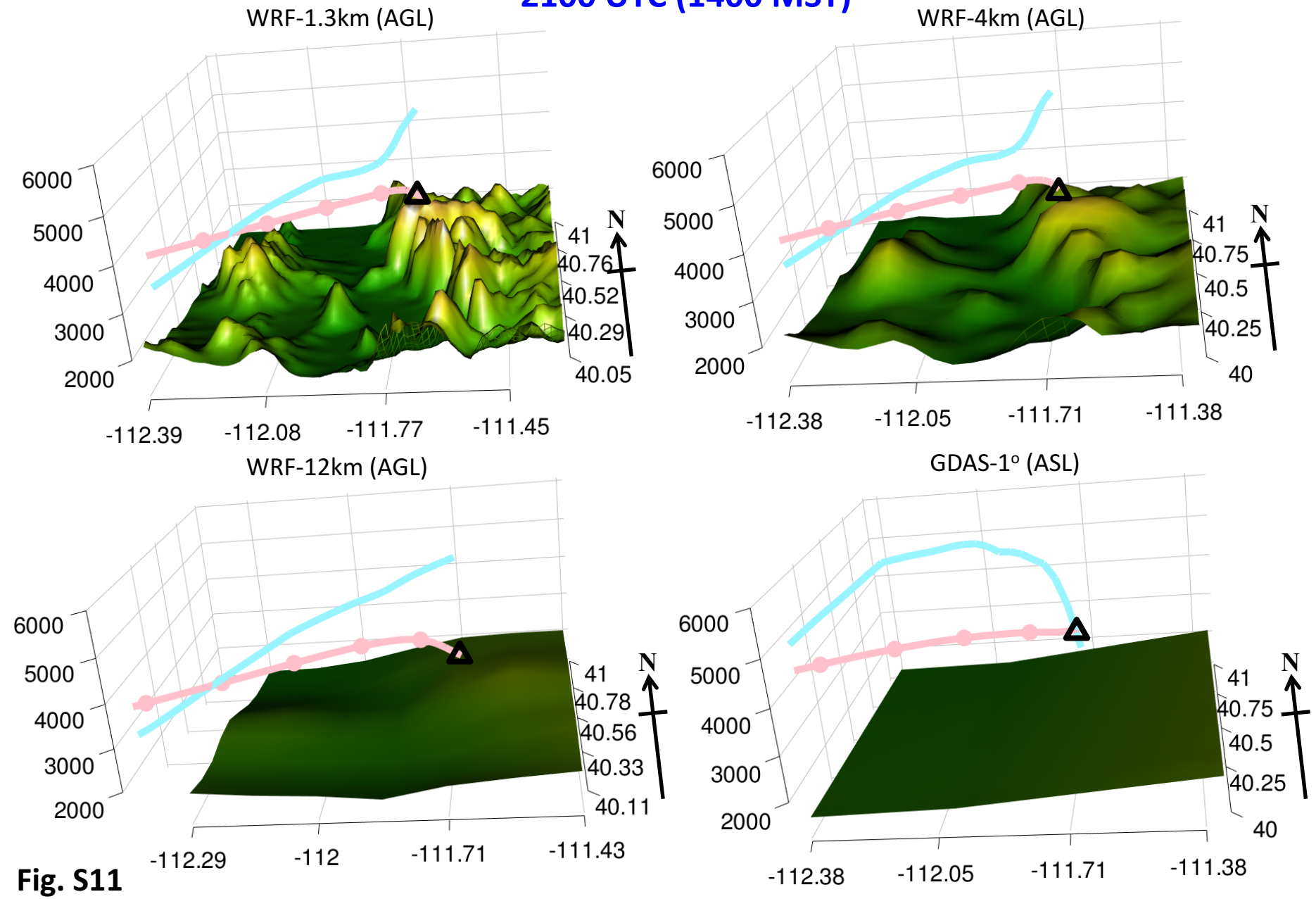

Fig. S11

SPL: Mean 3D Trajectory of Stochastic Particles & PBL ht for Different Runs

2100 UTC (1400 MST)

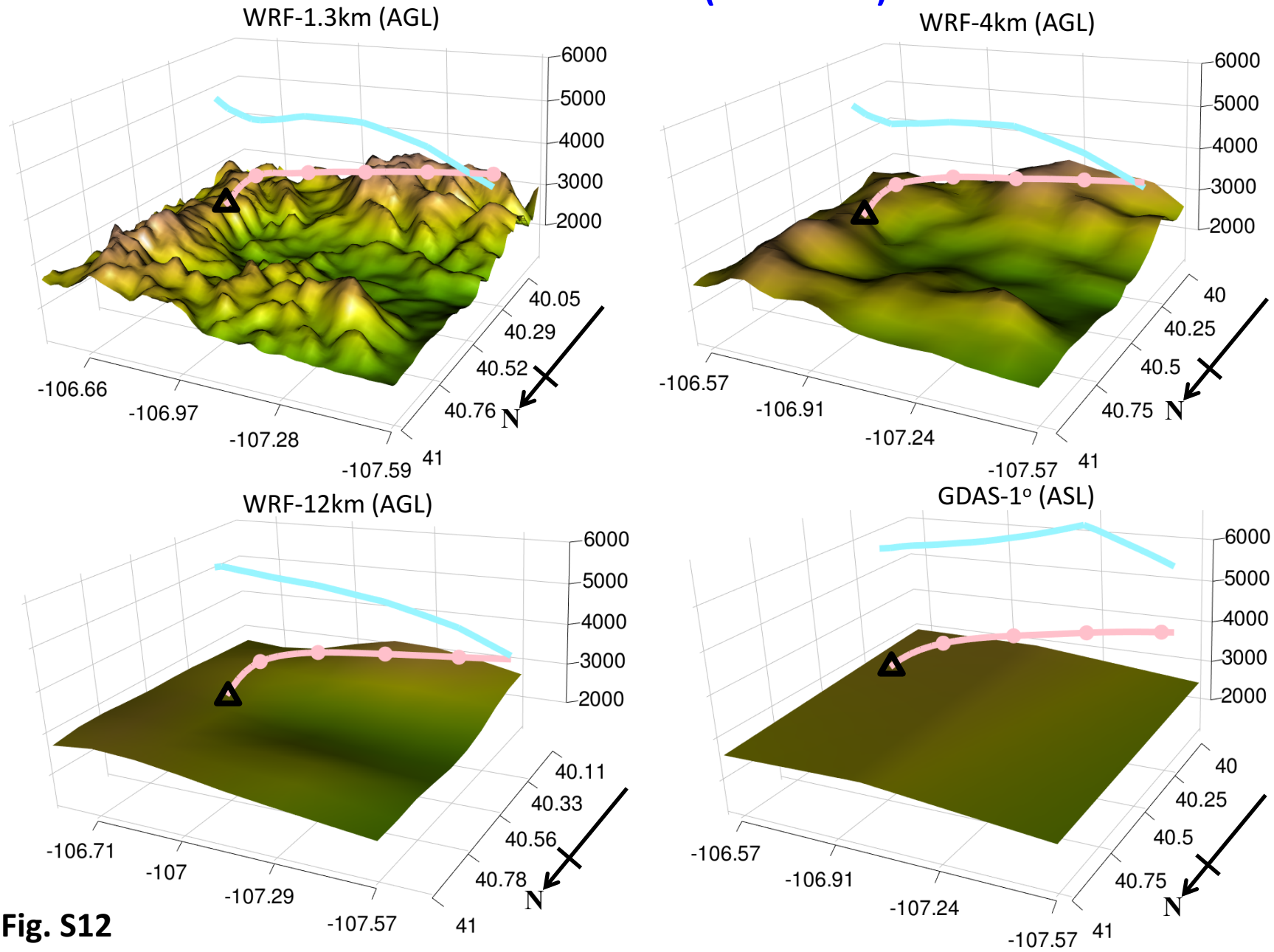

Fig. S12

NWR: Mean 3D Trajectory of Stochastic Particles & PBL ht for Different Runs

2100 UTC (1400 MST)

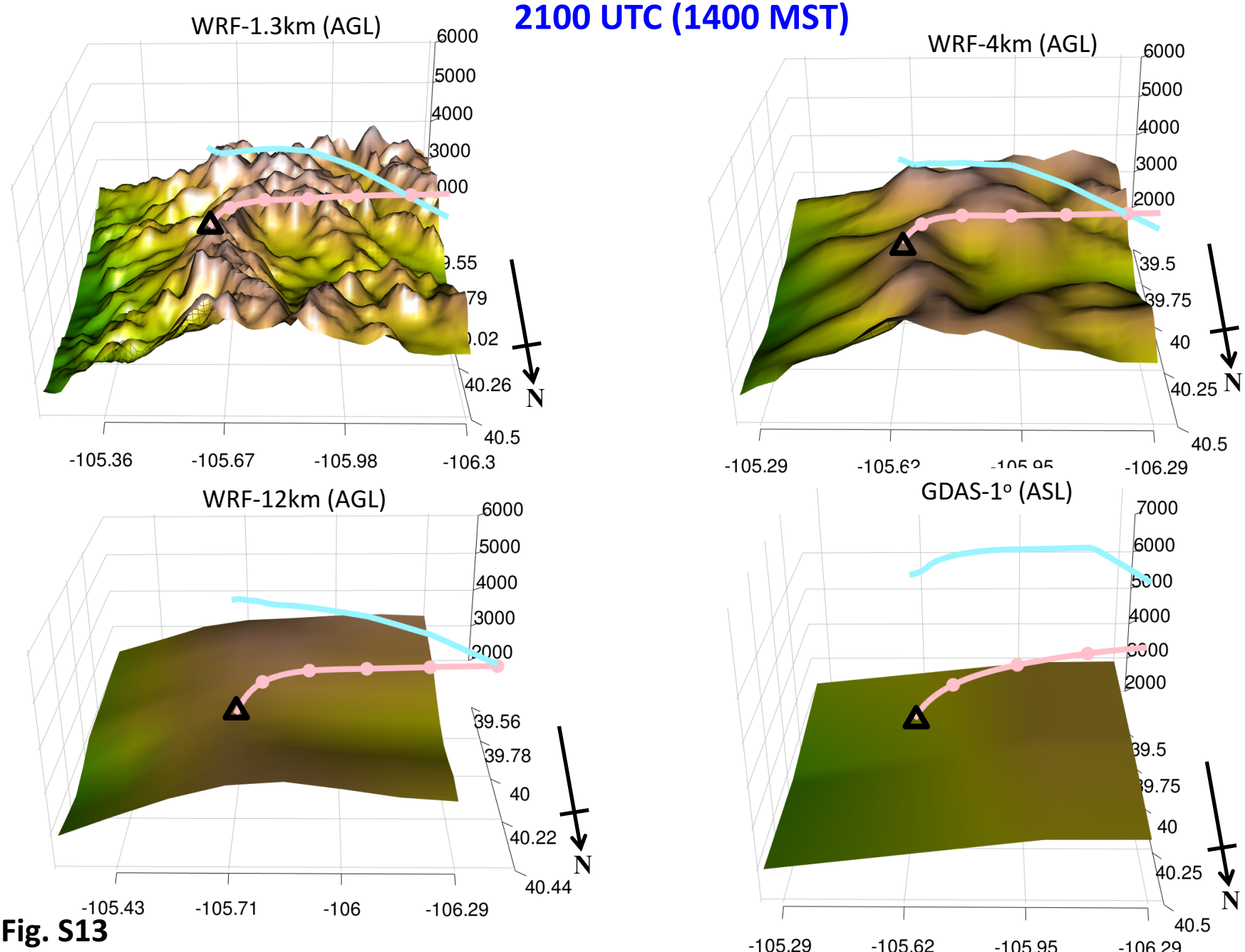

Fig. S13